

Concave Accretion Discs and X-ray Reprocessing

Eric G. Blackman, Theoretical Astrophysics, Caltech 130-33, Pasadena CA, 91125, USA
(submitted to MNRAS)

ABSTRACT

Spectra of Seyfert Is are commonly modelled as emission from an X-ray illuminated flat accretion disc orbiting a central black hole. This provides both a reprocessed and direct component of the X-ray emission as required by observations of individual objects and possibly a fraction of the cosmological X-ray background. There is some observational motivation to at least consider the role that an effectively concave disc surface might play: (1) a reprocessed fraction $\gtrsim 1/2$ in some Seyferts and possibly in the X-ray background, and (2) the commonality of a sharp iron line peak for Seyferts at 6.4KeV despite a dependence of peak location on inclination angle for flat disc models. Here it is shown that a concave disc may not only provide a larger total fraction of reprocessed photons, but can also reprocess a much larger fraction of photons in its outer regions when compared to a flat disc. This reduces the sensitivity of the 6.4KeV peak location to the inner disc inclination angle because the outer regions are less affected by Doppler and gravitational effects. If the X-ray source is isotropic, the reprocessed fraction is directly determined by the concavity. If the X-ray source is anisotropic, the location of iron line peak can still be determined by concavity but the total reflected fraction need not be as large as for the isotropic emitter case. The geometric calculations herein are applicable to general accretion disc systems illuminated from the center.

Key Words: accretion, accretion discs; line:profiles; galaxies: active; X-rays: galaxies; Xrays: stars

1. Introduction

Accretion discs are the standard paradigm to explain a wide variety of luminous galactic and extra-galactic accreting sources. Steady accretion requires dissipation of gravitational energy which produces the observed luminosity. Emission from X-ray binaries and active galactic nuclei (AGN) is thought to result from accretion onto a central massive black hole (e.g. Pringle 1981; Rees, 1984). The X-rays originate from the inner-most regions of the accretion flow and probe the associated dynamics and geometry.

X-ray spectra of Seyfert I AGN have been modeled by a combination of direct and reprocessed emission (see Mushotzsky et al. (1993) for a review). The direct component is from hot 10^9K electrons of optical depth ≤ 1 . The reprocessing component (e.g. Guilbert & Rees 1988; George & Fabian 1991) is composed of: 1) a Compton thick material in a moderate state of ionisation believed to be the thin accretion disc at $\leq 10^5\text{K}$, which produces iron fluorescence features and 2) possibly a Compton thin, highly ionised “warm absorber” which produces absorption features below 3 keV. If the disc extends to the inner stable orbit, a broad gravitationally red-shifted ~ 6.4 KeV iron K α fluorescence line can be produced. Material further inside can also contribute to the line (Reynolds & Begelman 1997) making a distinction between Kerr or Schwarzschild holes difficult (though see Young et al. (1998)). Generally, the iron line shape provides a diagnostic for strong gravity (Fabian et al., 1995; Tanaka et al 1996). Similar lines have also been seen in galactic black hole candidates. (Fabian et al. 1989; Done et al. 1992; Ebisawa 1996).

The best studied (post ASCA) iron line is that of MCG-6-30-15 (Tanaka et al 1995;

Iwasawa et al. 1996). Its profile varies with the continuum, but has been successfully modeled by reflection off of a flat Keplerian disc inclined ~ 30 degrees to the line of sight. However, ASCA has observed the ~ 6.4 KeV Iron lines in 22 Seyfert Is (Nandra et al. 1997) and as a population, they have a dispersion of only ± 3 degrees around 29 degrees in the predicted inclination angle when modelled with a flat disc. The peak of the line always appears at or near the rest frame 6.4KeV. Because the peak location is sensitive to the disc inclination angle in flat disc models (Laor 1991), the low dispersion is not expected for a distribution of randomly oriented discs—even in the presence of a dusty torus at large radii which narrows the angular range over which Seyfert Is, by class, are selected. The narrow iron line core near 6.4 KeV correlates with the intensity of the continuum flux when averaged over $\sim few \times 10^4$ seconds (Iwasawa et al. 1996). Perhaps this indicates a corresponding distance between the reprocessing region and the direct X-ray source.

A second issue is the ratio of total reprocessed to direct emission. In some Seyferts like MCG-6-30-15 this may slightly exceed 1 (Lee et al. 1998; Guainazzi et al. 1999), although for a population of 11 objects, the ratio seems to hover around 1 (Matt 1998). Some models of the cosmological X-ray background (c.f. Fabian 1992) also suggest that the reprocessed X-ray component may exceed the direct component by a ratio $\gtrsim 5$. If true, this might be explained by flat disc geometries by employing an anisotropic direct X-ray source through the inverse Compton process, (Ghisellini et al 1990; Rogers 1991), direct acceleration of electrons toward the disc (Field & Rogers 1993), source motion (Reynolds & Fabian 1997), or general relativistic (GR) effects (Martocchia & Matt 1996). But other possibilities, such as concavity, deserve investigation. It important to note however, that recent models of the

X-ray background (Comastri et al. 1995) do not require the reprocessed to direct emission ratio much different from 1.

A disc whose outer parts are thicker or concave with increasing height at larger radii may play a role in explaining the ubiquity of the iron line peak at 6.4KeV even if the total reprocessed to direct emission ratio inferred for a given object is of order 1. The concavity allows a larger fraction of the reprocessed emission to be reprocessed in the outer parts of the disc, away from the influence of the doppler and gravitational effects. The total reprocessed to direct fraction depends not only on the concavity but also on how isotropic the X-ray source is. For an isotropic X-ray source, the total reprocessed fraction will be large if concavity plays a strong role in determining where the iron line peak is. For an anisotropic source however, the concavity may play a strong role in determining where the iron line source is even if the total reprocessed fraction is modest.

Additional “concavity” beyond that of the simplest Shakura-Sunayev (Shakura 1973) discs can reflect a thickening disc with a flare due to the particular vertical structure and temperature profile (e.g. Keynon & Hartmann 1987 in the context of stellar discs.) Also, azimuthally dependent concavity can result from warping which may be tidally or radiatively driven (Terquem & Bernout 1993,1996; Pringle 1996,1997), or induced by a wind. Alternatively, the discs may incur a transition from a thick torus to a thin disc inward. Here I do not consider the dynamics in detail and just parameterize the concavity to highlight some simple effects related to the above observations. Concavity was considered by Matt et al. (1991) primarily for its effect on the iron line equivalent width, but this may

not be its most important role. In section 2, I explicitly derive the ratio of reprocessed to direct emission as a function of the curvature. Splitting the reprocessed contribution into components emanating from inside and outside a critical radius r_c , I then derive the ratio of contributions to the iron line from the outer (taken to be the “narrow component” around 6.4KeV) and inner regions (taken to be the “broad component”). The calculation results and line profile examples are discussed in section 3 and section 4 is the conclusion.

2. Concavity and the Reprocessed Emission

2.1 Basic Considerations

Here I take the direct X-ray source is taken to be an isotropic point emitter located above a Schwarzschild hole. (Later I will comment on the possibility of an anisotropic source.) The exact location of the X-ray source(s) is unknown. To marginally avoid considering reflection from material free-falling inside of radii $r = 6$ (Reynolds & Begelman 1997), I take the source height to be $H_e = 10$, where the r and H_e are in gravitational units of $R_g \equiv GM/c^2$, and M is the hole mass. Incident hard X-rays impinge onto the accretion disc and are scattered off an optically thin outer layer (see Matt et al. 1996). The X-ray photons also excite fluorescent photons from iron atoms. Below, the 6.4 KeV iron line flux is taken to be proportional to the incident flux. This assumes that the ionisation parameter is low enough over all $r \gtrsim 6$ to ensure cold iron line emission (Matt et al. 1996). The calculations then reduce to the geometry of Fig 1.

2.2 Total Reprocessed vs. Direct Flux Ratios for Concave discs

First consider the total reprocessed flux. The ratio of the observed flux in the reprocessed component to that in the direct component is the ratio of the number of photons which intercept the disc over the number of which escape directly. For the parameters chosen above, the GR effects are sub-dominant in all regions of the disc and comprise a maximum 30% correction. Note however, that GR leads to more flux impinging on the disc, so ignoring GR at first highlights a different way to achieve a high reprocessed fraction, and thus an overall lower limit.

In the Euclidean regime, the flux ratio of reprocessed to direct emission is given by the ratio of solid angle subtended by the disc to that subtended by the free space to the observer. The azimuthal angle drops out by symmetry. Take the disc's reprocessing layer to have a height

$$h(r) = a(r/6)^b \text{ [for } a(r/6)^b < r \text{] ; } r \text{ [for } a(r/6)^b > r \text{]}, \quad (1)$$

where the curvature index b implies concavity for $b > 1$, and $a \equiv h(r_{in})/r_{in}$ at the inner disc radius $r_{in} = 6$. The two regimes of (1) are imposed to enforce $h \leq r$ at all radii. The dashed curves of Fig. 2 show the b for which $h(r_{out}) = r$ for different outer radii r_{out} . The ratio of reprocessed to direct flux, using the angles shown in Fig. 1, is then

$$F_{rep}/F_{dir} = \frac{\int_{\pi/2 - \text{Tan}^{-1}[(H_e - h(r_{out}))/r_{out}]}^{\pi - \text{Tan}^{-1}[r_{in}/H_e]} \text{Sin}\theta d\theta}{\int_0^{\pi/2 - \text{Tan}^{-1}[(H_e - h(r_{out}))/r_{out}]} \text{Sin}\theta d\theta}. \quad (2)$$

For a strictly flat disc, the ratio is given by (2) with $h(r) = 0$, and then $F_{rep}/F_{dir} < 1$.

2.3 Concavity and the Reprocessed Iron Line

Consider two components to the reprocessed iron line, motivated partly by the approach employed for the best-studied MCG-6-30-15 example (e.g. Iwasawa 1996). Take

the first component to peak at the rest frame frequency and the second to be the remaining broad line. After choosing a core width, one can derive a corresponding critical radius, r_c , outside of which all the narrow core emission emanates. The role of concavity becomes apparent by comparing the flux ratios from the two disc regions for flat vs. curved discs.

Iwasawa et al (1996) and Nandra et al. (1997) consider a narrow component width $\sim \pm 2.5\%$ around the 6.4 KeV peak rest energy in MCG-6-30-15 and for the population of 22 objects respectively. We can estimate r_c by assuming that the spread corresponds to a Doppler width enveloping the largest and smallest frequencies at r_c . The Doppler shift at large r is

$$\nu/\nu_e \simeq (1 \pm \Delta v/c), \quad (3)$$

where ν is the frequency, ν_e is the rest frequency = 6.4keV, and Δv is the maximum spread in velocity. For Δv we take the Keplerian speed $\sim c(1/r)^{1/2}$, Thus

$$r_c \simeq (\Delta\nu/\nu_e)^{-2}, \quad (4)$$

where $\Delta\nu$ is the frequency half-width of the core. For $\Delta\nu = 0.025$, $r_c = 1600$, while for $\Delta\nu = 0.05$, $r_c = 400$.

Using Fig. 1 to calculate the ratio of flux emanating from outside r_c to that from within r_c we obtain

$$F_{out}/F_{in} = \frac{\int_{\pi/2 - \text{Tan}^{-1}[(H_e - h(r_c))/r_c]}^{\pi/2 - \text{Tan}^{-1}[(H_e - h(r_{out}))/r_{out}]} \text{Sin}\theta d\theta}{\int_{\pi/2 - \text{Tan}^{-1}[r_{in}/H_e]}^{\pi - \text{Tan}^{-1}[r_{in}/H_e]} \text{Sin}\theta d\theta}. \quad (5)$$

Notice from Fig. 1 that the angle bounds in the integral are the same regardless of whether $h(r_c) > H_e$ or $h(r_c) < H_e$. For a flat disc, (5) is found from taking $h = 0$ for all r .

2.3 Local Approach

The above approach is the simplest for the Euclidean case, but to include GR and actually compute line profiles, GR corrections are more easily incorporated in a formalism which integrates over r . An equivalent way to compute (5) is to note that the reprocessed line flux from an element of area dA is proportional to the impinging flux $f(r, H_e, h)$ at that radius projected onto the area dA (see Fig. 1)

$$dF \propto g_r(r)f(r, H_e, h)\text{Cos}\lambda r(dr^2 + dh^2)^{1/2} = g_r(r)f(r, H_e, h)\text{Cos}\lambda(1 + dh^2/dr^2)^{1/2}rdr$$

$$\propto g_r(r)(r^2 + (H_e - h)^2)^{-1}(1 + dh^2/dr^2)^{1/2}rdr, \quad (6)$$

where $f(r, H_e, h) \propto (r^2 + (H_e - h)^2)^{-1}$. The angle λ is between the normal to the area element and the X-ray source direction (Fig. 1) so that

$$\text{Cos}\lambda = \text{Cos}(\pi/2 - \text{Tan}^{-1}(dh/dr) + \text{Tan}^{-1}[(h(r) - H_e)/r]). \quad (7)$$

The quantity $g_r(r) = (1 - 2/r)^{-4}(1 - 2/r)^{1/2}(1 + z)^{-4}$ is the product of three correction factors to an otherwise Euclidean formula: The first is the Doppler + GR correction to the Euclidean illumination function as approximated by Reynolds & Begelman (1996). The second is the correction to the area measure in the integrand. The third factor $(1 + z)^{-4}$ is the red-shift correction. This is given by $(1 + z) = (p^\mu u_\mu)_{em}/E_{obs}$ where subscript em stands for emitted location (i.e. disc), E_{obs} is the photon energy measured by the observer, and $p^\mu u_\mu$ is the product of the photon 4-momentum and bulk motion 4-velocity along the sight line. At finite inclination angle, some of the photons from the inner regions populate the narrow core. In addition, some inner region photons may be lost as they impinge on

the outer disc and incur a second reprocessing. The formulae for a face on inner disc thus provide a lower limit to the ratio F_{out}/F_{in} for all inclination angles. From Reynolds & Begelman (1996), we then obtain $(1+z)^{-4} = (1-3/r)^2$. Notice that the illumination function correction and the red-shift correction compete. The former enhances, while the latter decreases the flux. The net effect is an increase in the redshifted component and an increase flux from the inner regions, and thus a decrease in (5). I ignore the tiny corrections to $g_r(r)$ which result from a finite h .

Using (7) in (6) gives

$$F_{out}/F_{in} = \frac{[\int_{r_c}^{r_{out}} g_r(r') dr' r' (1 + (\frac{dh}{dr'})^2)^{1/2} (r'^2 + (H_e - h)^2)^{-1} \text{Cos}\lambda(r')] }{[\int_{r_{in}}^{r_c} g_r(r') dr' r' (1 + (\frac{dh}{dr'})^2)^{1/2} (r'^2 + (H_e - h)^2)^{-1} \text{Cos}\lambda(r')]}. \quad (8)$$

For a flat disc, $dh/dr = 0$ and then $\text{Cos}\lambda = (H_e - h)/(r^2 + (H_e - h)^2)^{1/2}$. In the limit $g(r) = 1$ for all r , the results from using (8) are *identical* to those from (5). In the next section I discuss the results of the above ratios and show some line profiles.

3. Results, Line Profiles, and Discussion

The solid curves of Fig. 2 show F_{rep}/F_{dir} as a function of b for three values of r_{out} , using $a = 1/50$, $H_e = 10$, and $b \geq 1$. The restriction to concave curvature (i.e. $b > 1$) means that the entire disc surface sees the X-rays. The imposed restriction that $h \leq r$ leads to a maximum ratio of 5.4 in Fig 2. For the above parameters, a Euclidean flat disc would give only $F_{rep}/F_{dir} \sim 0.87$ for an isotropic source. Note that if the X-ray source were suitably anisotropic, the ratio F_{rep}/F_{dir} need not be significantly greater than 1 even for the optimal b . In that case, the Euclidean flat disc ratio for the same anisotropy would still be of order 5 times less for the optimal b .

Fig. 3 shows F_{out}/F_{in} , for different values of r_{out} and r_c . (To be conservative, Fig. 3 employs (8) in order to include the rough GR corrections which *lower* the curves relative to the Euclidean case, making the effect $\sim 30\%$ less pronounced. By contrast, for Fig 2, the conservative lower limit is given by the Euclidean equation (2)). There are two regions for each curve of Fig. 3. For low b , the gain from orientation toward the source wins over the decrease in flux from the extra distance to the disc at a given r and the curves rise. However since $H_e \ll r_c$, above the b at which $h(r)/r = 1$, the increasing distance between the X-ray point source and the disc for larger r wins and the curves then decline. A Shakura-Sunaejev (Shakura & Sunaejev 1973) disc corresponds to $b = 9/8$. For a flat disc the ratios are low: for $r_c = 400$, $F_{out}/F_{in} \sim 0.03$ and for $r_c = 1600$, $F_{out}/F_{in} \sim 0.007$.

The $r_c = 400$ solid curve lies completely above the $r_c = 1600$ solid curve in Fig. 3 since r_{out} is the same in both cases. This contrasts the dashed curves which address a different issue. The approximate $2 - 4 \times 10^4$ sec delay between an increase in continuum emission and the response of the narrow core line for e.g. MCG-6-30-15, (Iwasawa et al. 1996) motivates considering that some reprocessing material resides at the associated distance from the X-ray source. For a $10^7 M_\odot$ hole, this corresponds to a distance of $400 - 800 R_g$. The Keplerian velocities at this r_c are consistent with a few percent frequency width of the core. This motivates determining the amount of reprocessed emission coming from $r_c \lesssim r \lesssim 10r_c$ and the results are the dashed curves of Fig 3. Because of the narrow range in r , the curves are lower than for the solid curves but there is still a range of b for which such an outer “ring” can produce $F_{out}/F_{in} \gtrsim 1/3$, even for $r_{out} = 4000$, which is of order that required for MCG-6-30-15 (Iwasawa et al. 1996). By contrast, for flat discs from (2),

even the more favorable case ($r_{out} = 10r_c$, $r_c = 400$) gives only $F_{out}/F_{in} = 0.03$. The dashed curves in Fig. 3 cross because a decade in r_c for higher r_c is larger, but farther out, than a decade in r_c for lower r_c .

The fact that emission in the narrow peak could originate from large radii means that the ubiquity of observed peaks near 6.4keV in the 22 Seyferts studied by Nandra et al (1997) would not be as sensitive to the inner disc inclination angle. The maximum velocity dispersions at such large radii are small (e.g. $\Delta\nu \leq 5\%$ at $r = 400$). For a strictly flat disc, some tuning in inclination angle is required to produce the location of the observed peak because gravitational+transverse Doppler red, and blue shifts conspire to produce the particular peak values. Figure 4 shows some line profiles using the formulae of Fabian et al. (1989) (Esin 1998) but with a modified emissivity function to include the flat and concave disc cases. The emissivity function of Fabian et al. (1989) was $\epsilon \propto (r_{in}/r)^2$ and I replace this by the factor in (8): $(1 + (\frac{dh}{dr})^2)^{1/2}(r^2 + (H_e - h)^2)^{-1} \cos\lambda(r)$. This simplifies for a flat disc as discussed below (8). As expected from Figs. 2 and 3, Fig 4 shows the narrow peak at 6.4KeV for the value of $b = 1.7$ even at an inclination angle of 40deg. The effect weakens significantly for $b = 1.3$ as expected. Secondary reprocessing (Matt et al. 1991) of inner disc radiation by outer disc radiation is not considered. This would be less likely to effect the peak because the peak is produced from emission at large radii. Also, the constraint $h \leq r$ means angles of inclination $< 45\text{deg}$ are less affected by shadowing.

The above results show that for a range of b and r_{out} , the ratios F_{rep}/F_{dir} and F_{out}/F_{in} can be more than an order of magnitude larger than for flat discs. The concavity may

thus predominantly affect the total reprocessed fraction or the line shape rather than the line equivalent width (Matt et al. 1991). The results are not strongly sensitive to the parameters a , H_e , or r_{in} for $H_e, r_e \gtrsim 6$, but for $r_{in}, H_e < 6$ a more detailed inclusion of the ionisation fraction and shadowing is required.

The value of b which provides both the largest F_{out}/F_{in} and F_{rep}/F_{dir} for the range of r_{out} considered is $1.5 \lesssim b \lesssim 1.9$ out to the radius for which $h(r)/r = 1$. (The value $b \sim 1.5$ is that of an isothermal disc.) A disc which changes from a thin to thick disc/torus at $r \gtrsim r_c$ and has reprocessing material in the torus, may be approximated by (1). Some excess in reprocessed emission can also result from a warped disc, possibly tidally or radiatively driven (e.g. Terquem & Bertout 1993,1996; Pringle 1996,1997) or induced by wind torques, but the azimuthal dependence must then be considered (e.g. Terquem & Bertout 1993). The role of an anisotropic X-ray source would change the total reprocessed fraction, but not the influence on the line peak location, or the comparisons to a flat disc.

4. Conclusions

Some simple but pronounced effects of a concavely curved accretion disc are captured by estimating the total reprocessed vs. direct flux and the relative flux emanating from inside and outside of a critical radius r_c . For a range of b , the reprocessed flux from $r > 400$ and even $r > 1600$ can contribute significantly to a rest frame iron line peak even when the (X-ray) radiation source is at located at $H_e \sim 10$. This alleviates some sensitivity of disc model predictions (e.g. Laor 1991) to the disc inclination angle, as seen in Fig 4. Reprocessing at large distances also predicts a time delay between changes in the direct

continuum emission and the reprocessed emission which may be observed in some Seyferts (Iwasawa et al. 1996).

In addition, concave discs may produce $F_{rep}/F_{dir} \gtrsim 5$ for an isotropic X-ray source which provides another means for some AGN models of the X-ray background to account for the high required reprocessed fraction (c.f. Fabian 1992). However, if the X-ray background and Seyferts do not generically require a high reprocessed fraction (Comastri et al 1995; Matt 1998), the ubiquity of the iron line peak at 6.4 KeV could still be influenced by concavity when compared to a flat disc: The concavity affects not only the total reprocessed fraction for a given X-ray source anisotropy, but the relative reprocessed fraction from different parts of the disc. Finally, note that the disc could be curved or could change from a thin to a thick disc with entrained reprocessing material, such that the effective global reprocessing geometry is approximated by a concavity.

Acknowledgements: Many thanks to E. Chiang, C. Peres, and S. Phinney for discussions, to A. Esin for a subroutine, and to the referee for comments.

Comastri A., Setti G., Zamorani G. Hasinger G., 1995, A&A, 296, 1

Dermer C.D., 1986, ApJ, 307, 47

Dermer C.D., Liang E. P., Canfield E., 1991, ApJ, 369, 410

Done C. Mulcahaey J.S., Mushotzky R.F., Arnaud K., ApJ 395, 275.

Ebisawa K., 1996, in *X-ray Imaging and Spectroscopy of Hot Plasmas*, ed. F.Makino &

K. Matsuda, (Tokyo: Universal Academy Press) p427. Fabian A.C., Rees, M.J., Stella L., White N.E., 1989, MNRAS, 238, 729.

Esin A., personal communication.

Fabian A.C., et al., 1995, MNRAS, 277, L11.

Fabian, A.C., 1992, in *The X-ray Background* Barcons, X. and Fabian, A.C. eds., (Cambridge: Cambridge Univ. Press), p305.

Fabian A.C., George I.M., Miyoshi, S., Rees, M.J., 1990, MNRAS, 240, 14P.

Field G.B. & Rogers, R.D., 1993, ApJ 403, 94.

Galeev A.A., Rosner R., Vaiana G.S., 1979, ApJ, 229, 318

Ghisellini G., George I.M., Fabian A.C., Done C., MNRAS, 1990, 248, 14.

Guilbert P.W. & Rees. M.J., 1988, MNRAS 233, 475.

Guainazzi M. et al., 1999, A&A, 341, L27.

Haardt F., Maraschi L., 1993, 413, 507

Iwasawa K. et al., 1996, MNRAS, 282, 1038

Kenyon S.J. & Hartmann L., 1987, ApJ, 323, 714.

Laor A., 1991, ApJ, 376, 90

Livio M. & Pringle, J.E, 1996, 278, L35.

Lee J.C., Fabian, A.C., Reynolds, C.S., Iwasawa, K. & Brandt, W.N., 1998, MNRAS, 300, 583.

Martocchia A., Matt G., 1996, MNRAS, 282, L53.

Matt G., 1998, astro-ph/9811053.

Matt G., Fabian A.C., Ross R.R, 1996, MNRAS, 278, 111.

Matt G., Perola G.C., Piro, L., 1991, A& A, 247, 25.

Mushotzky R.F., Done C.; Pounds K.A., 1997, ARA&A, 31, 717

Nandra K., George I.M., Mushotzky R.F., Turner T.J., Yaqoob T., 1993, ApJ, 477, 602

Pringle J.E., 1996, MNRAS, 281, 357.

Pringle J.E., 1997, MNRAS, 292, 136.

Rees M.J., 1984, ARAA, 22, 471.

Reynolds, C.S. & Begelman, M.C., 1997, ApJ, 488, 109.

Reynolds, C.S. & Fabian, A.C., 1997, MNRAS, 290, L1.

Rogers, R.D. & Field G.B., 1991, ApJ, 370, L57.

Rogers R.D. 1991, ApJ, 383, 550.

Shakura, N.I. & Sunyaev R.A., 1973, A& A, 24, 337.

Tanaka, Y. et al., 1995, Nature 375, 659.

Terquem C. & Bertout B., 1993, A&A, 274, 291.

Terquem C. & Bertout B., 1996, MNRAS, 279, 415

Young, A.J., Ross, R.R. & Fabian, A.C., 1998, MNRAS, 300, 11.

Zdziarski A.A., Fabian A.C., Nandra K., Celotti A., Rees M.J., Done C., Coppi P.S.,
Madejski G.M., 1994, MNRAS, 269, L55

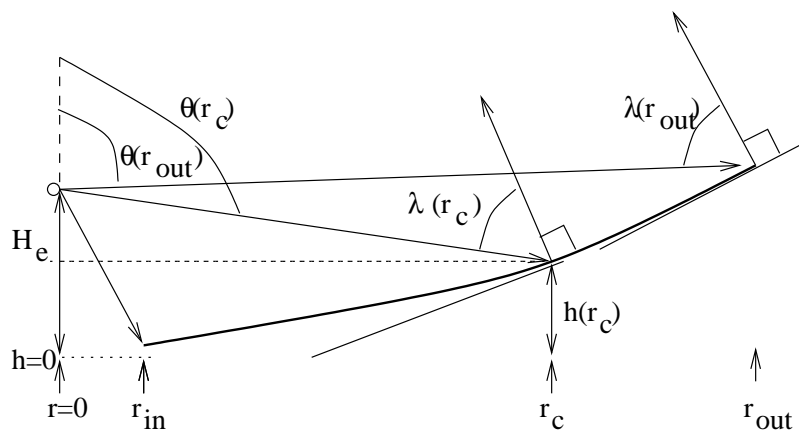
Zdziarski A.A., Johnson W.N., Done C., Smith D., McNaron-Brown K., 1995, ApJ, 438,
L63

Figure 1 Caption: Schematic of X-ray source (small circle) above disc surface (thick black curve). Two values of $\theta(r)$ and $\lambda(r)$ angles are shown for illustration as used in (2), (5) and (8). Regime (a) $H_e < h$, and (b) $H_e > h$.

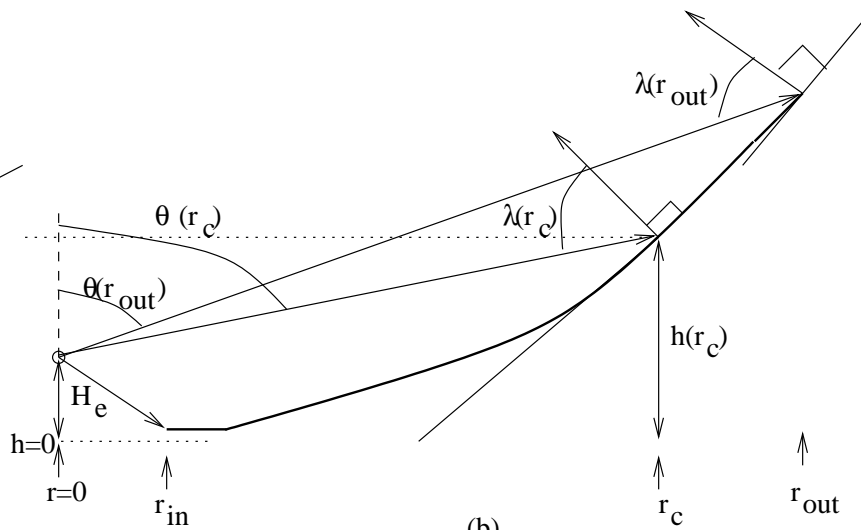
Figure 2 Caption: Plot of $h(r)/r$ (dashed curves) and F_{rep}/F_{dir} (solid curves) vs. b for $r_{out} = 10^5, 16000, 4000$ from left to right in each curve group. Values of $H_e = 10$, $r_{in} = 6$, and $a = 1/50$ are used in all curves. The flattening is the result of imposing $h(r) \leq r$ for all r in (1). The X-ray source is assumed to be isotropic for this graph. Simple anisotropies could be included by multiplying the y-axis by a constant fraction.

Figure 3 Caption: F_{out}/F_{in} vs. b from (8) for $r_{out} = 10^5$ (solid curves) and $r_{out} = 10r_c$ (dashed curves). The top solid and dashed curves as measured at $b = 1$ have $r_c = 400$, and the bottom curves have $r_c = 1600$. The dashed curves cross and merge with the solid curves above the b for which $h(r)/r = 1$. The condition $h(r) \leq r$ is imposed, but the presence of the down-turns only requires $r_c \gg r_{in}$.

Figure 4 Caption: Line profiles for flat and concave models based on Fabian et al. (1989) with $r_{out} = 10^4$ with emissivity function modified as discussed in text. Solid lines are for flat discs at inclination angles of 40 deg (broader curve) and 30 deg (narrower curve) respectively. The concave disc curves match onto the wings of the flat curves. There are 4 curved disc profiles signaturred by the height of their peaks. The largest has $b = 1.7$ and 30 deg inclination. The next largest is $b = 1.7$ and 40 deg. The next is $b = 1.3$ and 30 deg, and the lowest is $b = 1.3$ and 40 deg.



(a)



(b)

